ACS Energy LETTERS

http://pubs.acs.org/journal/aelccp

LETTER

Discordant Gd and Electronic Band Flattening Synergistically Induce High Thermoelectric Performance in n-type PbTe

Moinak Dutta, Raju K. Biswas, Swapan K. Pati, and Kanishka Biswas*

Cite This: *ACS Energy Lett.* 2021, 6, 1625−1632

Read Online

ACCESS | Metrics & More | Article Recommendations | Supporting Information

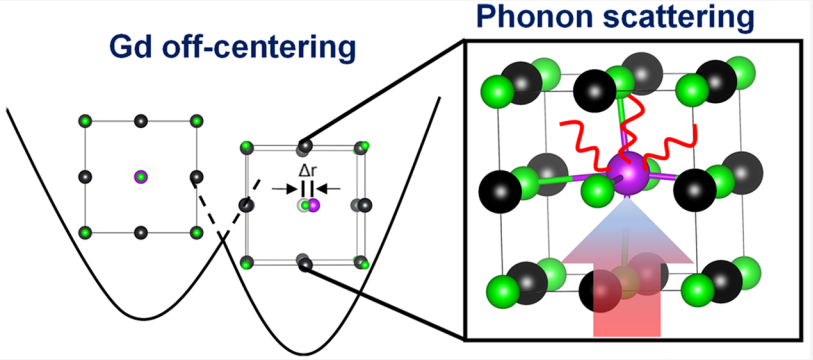

ABSTRACT: p-type PbTe is the most sought-after material in thermoelectrics due to its ultrahigh thermoelectric figure of merit (zT), but the performance of n-type PbTe lags behind due to the simplicity of its conduction band compared to those of rich valence bands. Here, we have synergistically enhanced the Seebeck coefficient and lowered the lattice thermal conductivity of n-type PbTe by Gd doping, which resulted in high thermoelectric performance. Gd doping in PbTe enhances the electron effective mass via flattening of the conduction band, which significantly improves the Seebeck coefficient. Gd is found to remain in an off-centered position inside the rock-salt PbTe lattice, which increased the lattice anharmonicity. Density functional perturbation theory (DFPT) calculations indicate that Gd induces a low energy nearly flat optical phonon mode that drastically increases the phonon scattering rate and lowers lattice thermal conductivity to 0.78 W/(m K). As a result, we achieved a high zT of 1.65 at 678 K for $Pb_{1-x}Gd_xTe_{1-y}I_y$ (x = 0.33%, y = 1%).

The current technological advancement allows us to convert only a fraction of resources into efficient energy (like electricity), and a major part (∼65%) is lost as heat during the conversion. Thermoelectric materials, which can directly and reversibly convert waste heat to electricity, are thus seen as a potential candidate in energy management.[1−5] The performance of the thermoelectric materials is given by its dimensionless figure of merit, zT, which is expressed as $zT = \frac{\sigma S^2}{\kappa}T$, σ, S, and κ being the electrical conductivity, the Seebeck coefficient, and the total thermal conductivity, respectively. While σ is governed by charge carriers in a material, the thermal conductivity propagates due to both charge carriers (κ_{el}) and lattice vibrations (κ_{lat}). The complicated inter-relationship of the thermoelectric parameters (σ, S, and κ_{el}) lends a major bottleneck in improving zT. Hitherto, most of the improvements in thermoelectric materials have primarily focused on balancing these interdependent parameters.[1] Several state of the art strategies like electronic band flattening,[6,7] band convergence,[8,9] charge carrier optimization,[10−12] resonant states,[13,14] band alignment,[15,16] mobility enhancement,[17,18] effective mass engineering,[6,19,20] slight symmetry reduction,[21,22] etc. have been effectively carried out to improve the power factor (σS^2) of a material.[23] Similarly, lowering the κ_{lat} of a material also garnered several novel approaches, e.g., phonon scattering by point defects,[6,24,25] nano precipitates,[15,26−28] all scale hierarchical phonon scattering,[29−31]

Received: February 28, 2021
Accepted: March 26, 2021
Published: March 31, 2021

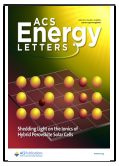

https://doi.org/10.1021/acsenergylett.1c00450
ACS Energy Lett. 2021, 6, 1625−1632

and intrinsic phonon prohibiting pathways,[32] which have been successfully implemented until date.

PbTe adopts a rock salt structure, which is known for its unprecedented p-type thermoelectric performance in the temperature range 700−950 K. High performance in p-type PbTe originates due to its intrinsic low thermal conductivity arising from significant lattice anharmonicity and presence of unique electronic band structure.[33] The valence band (VB) of PbTe is composed of two neighboring bands L and Σ, which have very little energy offset ($\Delta E_{L\text{-}\Sigma}$ = 0.15−0.20 eV)[33] and thus effective valence band convergence has been realized in p-type PbTe to improve upon its thermoelectric performance.[8,9,30,34] On the other hand, the conduction band (CB) of PbTe is composed of only a single L band and thus it is lagging to match the performance of its p-type counterpart.[33,35] The presence of lower degenerate valleys in CB as compared to VB generates intrinsically low n-type Seebeck coefficient values and thus poses a greater challenge to improve its n-type thermoelectric performance.[33,35]

Recent progress on n-type PbTe primarily focuses on optimizing charge carrier concentration and mobility,[6,17,18,36,37] simultaneously modulating the electronic and thermal properties in PbTe-Cu_2Te[17] and PbTe-$AgSbSe_2$,[38] and enhancing band effective mass as in the case of $Pb_{0.988}Sb_{0.012}$Te-GeTe,[19] $Pb_{0.98}Ga_{0.02}$Te-GeTe,[20] and PbTe-MnTe.[6] Similarly, nanostructuring to reduce κ_{lat} and simultaneously improve electronic properties is also observed In- and Sb-codoped PbTe,[26] PbTe-PbS,[7] etc.[39,40] However, the simplicity of the conduction band and a large band offset between two neighboring conduction bands ($\Delta E_{L\text{-}\Sigma} \sim$ 0.45 eV) prohibited n-type PbTe from being as efficient as its p-type counterpart.[33,35]

Herein, we demonstrate superior n-type thermoelectric performance for Gd-doped PbTe in the temperature range 295−823 K. $Pb_{1-x}Gd_x$Te (x = 0.33%) exhibits an zT of ∼1.2 at 783 K, and with subsequent n-type electrical transport optimization with iodine (I) doping, the maximum zT reaches a high value of ∼1.65 at 678 K for $Pb_{1-x}Gd_xTe_{1-y}I_y$ (x = 0.33%, y = 1%), which is among the highest values reported for n-type PbTe. Gd is an n-type dopant and even 0.25 mol % Gd doping on PbTe increases the n-type carrier concentration to 1.46 × 10^{19} cm^{-3}. Electronic structure analysis through density functional theory (DFT) shows that upon Gd doping the principal band gap at the L point opens up along with formation of a noninteracting nearly flat conduction band, which increases the band effective mass (m^*). Atom projected electronic density of states (pDOS) reveals that the noninteracting band is contributed from the hybridized state of Gd, which enhances the Seebeck coefficient in Gd-doped PbTe. Furthermore, Gd is seen to remain in an off-centered position in the PbTe lattice due to the discordant nature of Gd in the octahedral coordination, which creates significant lattice anharmonicity. Phonon dispersion revealed the presence of a low-frequency nearly flat optical localized phonon mode. Both these effects, i.e., the presence of locally off-centered Gd in PbTe and the formation of a low-energy localized phonon mode, synergistically aid in enhancing the scattering of acoustic phonons. This significantly lowers the κ_{lat} of $Pb_{1-x}Gd_x$Te (x = 0.33%) to 0.78 W/(m K) at 735 K. Low κ_{lat} in n-type Gd- and I-codoped PbTe coupled with the electronic structure modification results in superior thermoelectric performance, and importantly, an impressive average zT (zT_{ave}) of 1.15 is obtained in the temperature range of 423−823 K.

High-quality polycrystalline $Pb_{1-x}Gd_x$Te (x = 0.25−0.75%) samples were synthesized using a vacuum-sealed tube melting reaction followed by spark plasma sintering (SPS) (see details in the Supporting Information). Like its parent sample all the doped samples crystallized in rock-salt structure (Figure S1a). Powder X-ray diffraction (PXRD) of all the samples shows no secondary phases within the detection limit of the instrument, indicating complete solubility of Gd into PbTe lattice (Figure S1b). Upon Gd doping, we observe a slightly shift in the PXRD peaks toward higher 2θ, indicating a decrease in the lattice parameter (Figures S1c and S2), which is due to the smaller ionic radius of Gd^{3+} (1.07 Å) as compared to that of Pb^{2+} (1.33 Å). Field emission scanning electron microscopy (FESEM) done in backscattering electron (BSE) mode and transmission electron microscopy (TEM) on $Pb_{1-x}Gd_x$Te (x = 0.33%) further confirms the absence of secondary phase precipitates and it is consistent with our PXRD data (Figures S3a and S4). Elemental color mapping during energy dispersive X-ray (EDAX) of the FESEM imaging shows that all the three atoms, i.e., Pb, Te, and Gd, are distributed homogeneously over the observed area (Figure S3c).

Gd is a n-type donor with a common oxidation state of +3, and upon substituting Pb^{2+}, it will impart an additional electron into the lattice. Previous low-temperature electronic transport measurement on Gd-doped PbTe showed similar n-type behavior.[42,43] An increase in the dopant concentration will thus lead to an increase in the n-type carrier concentration and hence subsequent enhancement in the electrical conductivity (σ). Upon Gd doping, the n-type carrier concentration of PbTe increases from 1.46 × 10^{19} cm^{-3} for $Pb_{1-x}Gd_x$Te (x = 0.25%) to 4.30 × 10^{19} cm^{-3} for $Pb_{1-x}Gd_x$Te (x = 0.75%) at room temperature (Table S1). Such an increase in carrier concentration is also observed in σ as it increases from 1020 S/cm for $Pb_{1-x}Gd_x$Te (x = 0.25%) to 2484 S/cm for $Pb_{1-x}Gd_x$Te (x = 0.33%) and finally to 2731 S/cm for $Pb_{1-x}Gd_x$Te (x = 0.75%) at ∼300 K (Figure 1a). With increasing temperature, we observe that σ decreases for all the samples as it is expected for degenerate semiconductors. Similarly, the Seebeck coefficient (S) for Gd-doped PbTe at ∼300 K decreases systematically from −111 μV/K for $Pb_{1-x}Gd_x$Te (x = 0.25%) to −72 μV/K for $Pb_{1-x}Gd_x$Te (x = 0.75%) (Figure 1b). The negative sign indicates its n-type conduction and agrees with the negative Hall coefficients. Temperature-dependent S increases with an increase in temperature with the highest S value of −261 μV/K obtained for $Pb_{1-x}Gd_x$Te (x = 0.25%) at 817 K. As a result, we obtained a high power factor of ∼24.7 μW/(cm K^2) at 483 K for $Pb_{1-x}Gd_x$Te (x = 0.33%) (Figure 1c).

To investigate the cause for such an enhanced power factor for Gd-doped PbTe, we plot the room temperature Seebeck coefficient as a function of carrier concentration (n). The resulting relationship when plotted against the theoretical single-band Pisarenko plot with varying effective mass (m^*) (m^* = 0.30m_e, 0.35m_e, 0.42m_e), indicated an increase in effective mass with an increase in Gd incorporation (Figure 1d). The effective mass for $Pb_{1-x}Gd_x$Te (x = 0.25%) is ∼0.35m_e, which increases to ∼0.45m_e for $Pb_{1-x}Gd_x$Te (x = 0.75%) and is comparable to that of PbTe-MnTe[6] but is higher than the effective masses for PbTe-PbS (∼0.32m_e),[7] PbTe:I (∼0.25m_e),[41] La-doped PbTe (∼0.33m_e),[39] PbTe-Cu_2Te,[17] GeTe alloyed $Pb_{0.988}Sb_{0.012}$Te (∼0.40m_e),[19] etc. This enhanced m^* dictates the high Seebeck coefficient for Gd-doped PbTe and influences the n-type thermoelectric performance in PbTe.

https://doi.org/10.1021/acsenergylett.1c00450
ACS Energy Lett. 2021, 6, 1625−1632

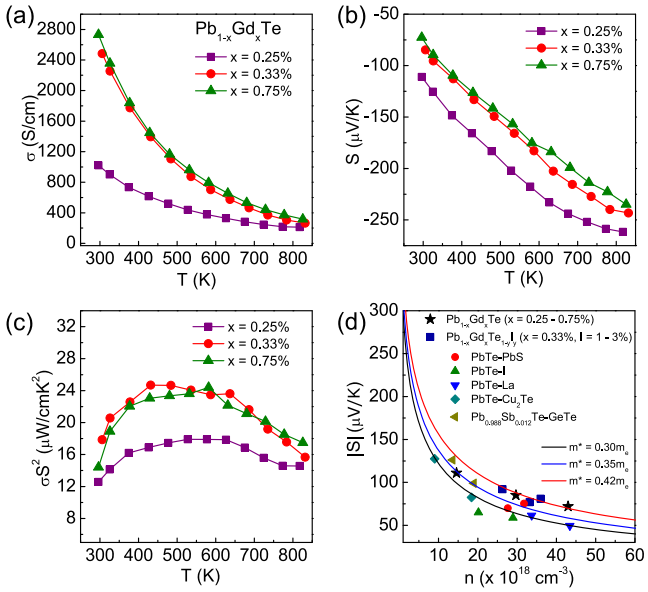

Figure 1. Temperature-dependent (a) electrical conductivity (σ), (b) Seebeck coefficient (S), and (c) power factor (σS^2) for Gd-doped PbTe samples. (d) |S| vs n plot for $Pb_{1-x}Gd_xTe$ (x = 0.25−0.75%) and $Pb_{1-x}Gd_xTe_{1-y}I_y$ (x = 0.33%, y = 1−3%) and plotted against the theoretical Pisarenko plot (solid lines) using the single band model with varying effective masses (m^*) of 0.30, 0.35, and 0.42 m_e and compared with previous results for PbTe-PbS,[7] PbTe:I,[41] PbTe:La,[39] PbTe-Cu_2Te,[17] and $Pb_{0.988}Sb_{0.012}$Te-GeTe.[19]

To understand how Gd doping influences the electronic transport properties of PbTe, we have performed DFT analysis of electronic structure. Figure 2a represents the electronic band structures of PbTe and Gd-doped PbTe plotted together for comparison. It is evident that upon Gd incorporation the band gap at L point opens up from 0.15 to 0.25 eV and is in line with the experimentally observed band gap opening upon Gd doping in PbTe (Figure S1d). Experimentally pristine PbTe has a band gap of ∼0.27 eV that increases to 0.29 eV for $Pb_{1-x}Gd_xTe$ (x = 0.75%). Furthermore, doping with Gd atoms introduces new features in the electronic band structure, which is beneficial for thermoelectric power factor. We observe a noninteracting single band just above the Fermi level in the conduction band that is nearly dispersionless around the Γ point and relatively dispersive along the L → Γ direction (red lines, Figure 2a). In fact, the flat nature is further verified through the sharp peak observed in the electronic DOS plot, which is shown by the purple arrow in Figure 2b and resembles that of Sb- and I-codoped PbTe.[24] Here, this nondispersive band leads to a higher Seebeck coefficient.[44,45] This band flattening is accompanied by an increase in the effective mass (m^*) of the conduction band. Pristine PbTe has an effective mass of ∼0.3m_e, which increases to ∼0.42m_e for Gd-doped PbTe and correlates closely with our modeled |S| vs n Pisarenko relationships (Figure 1d).

Atom projected electronic density of states (pDOS) for Gd-doped PbTe, revealed that the conduction bands are contributed by hybridized states of Te−Gd and Te−Pb bonding, with Pb showing the maximum contribution (Figure S5a). The electronic structures are calculated on the basis of the energetically most favorable configuration where Gd atoms are displaced along the crystallographic direction [111] from their ideal octahedral positions (Figure 2c). The off-centering of the Gd atom from the regular octahedral site is around 0.21 Å. This tendency of Gd to off-center from the parent Pb position might arise due to the discordant nature of Gd, which prefers to attain a higher coordination number (CN) (CN > 6) than possible for rock-salt PbTe (CN = 6).[46] Through the off-center configuration in Gd-doped PbTe, the structure further reduces their total energy significantly by 13 meV, which is shown in Figure 2d.

To further understand the chemical aspect of such Gd off-centering, we perform crystal orbital Hamitonian population (COHP) analysis between the orbitals of Te and Gd. COHP is calculated by considering the DOS multiplied by the Hamiltonian matrix element, and it indicates degree of covalency and nature of bonding interactions. A negative value of COHP signifies bonding nature while a positive value implies antibonding nature. Panels b and c of Figure S5 represent the COHP between the orbital of Te and Gd for both the undistorted (at regular octahedral site) and off-centered site of the Gd atom in the PbTe lattice, respectively. Interestingly, the interaction between Te and Gd orbitals is antibonding in nature above the Fermi level when Gd atoms are placed at their undistorted octahedral site. However, through the off-centering, the Gd−Te interaction becomes bonding in nature, which is energetically more favorable than the undistorted case. This locally off-centered Gd atoms increases the lattice anharmonicity and subsequently plays an important role in reducing lattice thermal conductivity of n-type PbTe significantly (discussed later).[20,47,48]

To comprehend the nature of thermal transport in these materials, we have calculated the phonon dispersion of pristine PbTe and Gd-doped PbTe (Figure 2e,f). We have observed that Gd atom introduces nearly a flat band around the frequency ∼38 cm^{-1} along Γ → Z → R → X directions over the Brillouin zone of phonon dispersion (Figure 2f). The low-energy nearly dispersionless optical mode reflects a weak interatomic force constant (IFC) and thereby reflects weak bonding between the associated atoms. These disentangled nondispersive optical phonons mode behave similarly to the Kondo-like phonon mode (details in methods), as seen previously for type-I clathrates with Ce and La as guests, and are doubly degenerate in nature (Figure S6).[49] These nondispersive degenerate phonon modes strongly scatter acoustic phonon modes, as is evident from the phonon−phonon anharmonic scattering rates, which increase a few fold (∼10^5 1/ps) at the frequency ∼38 cm^{-1} (Figure 2i). Here, the localized phonon mode shows larger scattering rates than that of other highly anharmonic compounds.[50,51] Moreover, we observe an avoided crossing between the longitudinal acoustic (LA) mode and the low energetic optical mode at 40 cm^{-1} near the high-symmetry S point in the phonon dispersion curve (Figure 2f). Such an avoided crossing is a signature for strong scattering of heat carrying acoustic phonons. Panels g and h of Figure 2 represent phonon DOS for PbTe and Gd-doped PbTe. A sharp peak in the density of states near 38 cm^{-1} (black arrow, Figure 2h) is evidenced due to the appearance of nondispersive flat optical phonon mode.

To uncover how this localized optical phonon mode affects the thermal transport, we have calculated the atom-projected phonon DOS (Figure S7a). The atom-projected phonon DOS of Gd overlaps significantly with Pb atoms and hybridizes less with Te atoms at ∼38 cm^{-1}. Furthermore, the Eigen mode visualization of this flat phonon mode shows significant contribution of the Gd atoms, indicating that the chemical origin of this flat phonon mode arises due to the doping of Gd

https://doi.org/10.1021/acsenergylett.1c00450
ACS Energy Lett. 2021, 6, 1625−1632

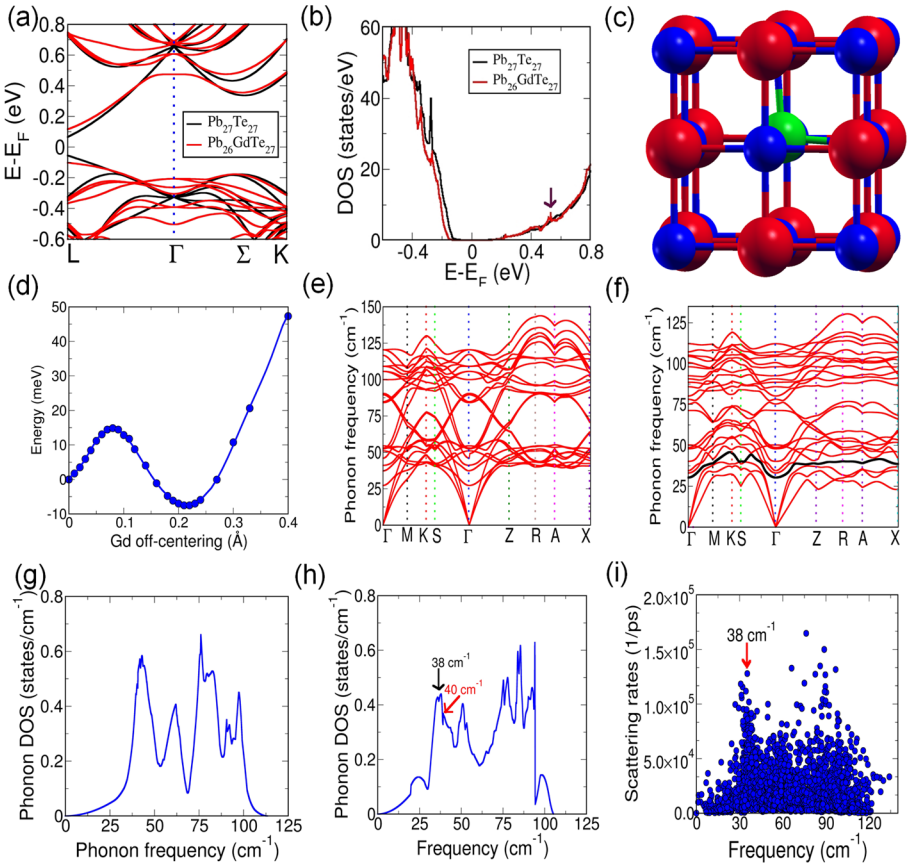

Figure 2. (a) Electronic band structure of PbTe (black) and Gd-doped PbTe (red), containing 54 atoms in the 3 × 3 × 3 supercell. (b) Electronic DOS of PbTe and Gd-doped PbTe. The relatively flat nature in the conduction band is further confirmed by a sharp peak in DOS, marked by a purple arrow. (c) Off-centered Gd atom at the distorted octahedral position in PbTe. Color codes are represented as follows: Pb, red; Te, blue; Gd, green. (d) Energy vs Gd off-centering plot showing a minimum energy when Gd is off-centered by ∼0.21 Å along the [111] direction. Phonon dispersion for (e) PbTe and (f) Gd-doped PbTe. Appearance of a special band, which is represented by black color, reveals nearly nondispersive nature along Γ → Z → R → X directions due to Gd doping. Phonon DOS for (g) PbTe and (h) Gd-doped PbTe. Here, a sudden enhancement in DOS at 38 cm^{-1}, which is indicated by a black arrow, appears because of Gd doping in PbTe. This increment in DOS originated because of a low-energy nearly flat band (shown in black color in Figure 2f) in the Gd-doped PbTe. (i) Anharmonic scattering rates as a function of frequency at T = 700 K. High values of scattering rates have been observed at frequency ∼38 cm^{-1}.

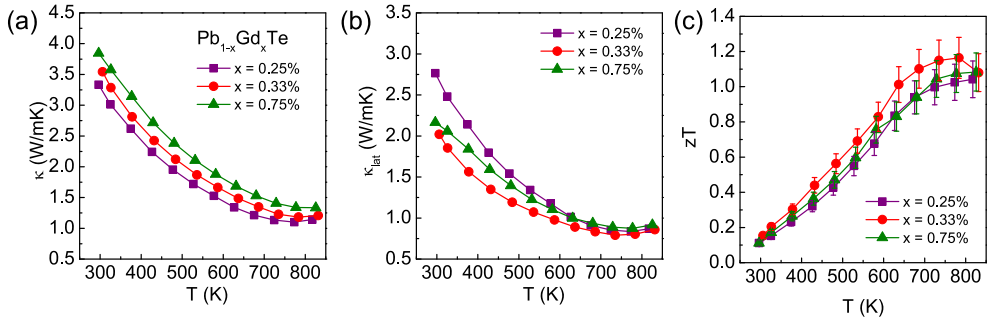

Figure 3. Temperature-dependent (a) total thermal conductivity (κ), (b) lattice thermal conductivity (κ_{lat}), and (c) thermoelectric figure of merit (zT) of Gd-doped PbTe samples.

atom in PbTe (Figure S6). These hybridized modes effectively scatter acoustic phonons and reduce lattice thermal conductivity significantly. Moreover, this localized optical mode reveals very low group velocity ∼230 m/s along Γ → Z → R → X directions (Figure S7b). The large scattering rates in combination with low group velocity driven by the low-energy localized optical mode is the primary reason to achieve low lattice thermal conductivity in Gd-doped PbTe. Gd doping further decreases the speed of sound along one of the transverse directions (v_t2) from 1690 to 1160 m/s (Table S2). This reduction in v_t2 decreases the overall mean speed of sound of the acoustic phonons from 1570 m/s for Gd-doped PbTe compared to 2035 m/s for pristine PbTe. This reduction in the mean speed of sound along with the presence of low-energy flat optical phonon mode and lattice anharmonicity

https://doi.org/10.1021/acsenergylett.1c00450
ACS Energy Lett. 2021, 6, 1625−1632

induced via Gd off-centering plays a pivotal role in lowering the κ_{lat} of Gd-doped PbTe.

The total thermal conductivities (κ) of these Gd-doped PbTe samples are shown in Figure 3a. The total thermal conductivity value at ~300 K for $Pb_{1-x}Gd_xTe$ (x = 0.25%) is 3.3 W/(m K), while for $Pb_{1-x}Gd_xTe$ (x = 0.33%) and $Pb_{1-x}Gd_xTe$ (x = 0.75%) the values are 3.5 and 3.8 W/(m K), respectively at the same temperature. The increase is mainly attributed to the increase in the electrical conductivity of the material with Gd doping, which increases the electrical thermal conductivity (κ_{el}). The lattice thermal conductivity (κ_{lat}), however, is seen to decrease initially when Gd doping is changed from 0.25 mol % to 0.33 mol % but increases for 0.75 mol % doping. κ_{lat} for $Pb_{1-x}Gd_xTe$ (x = 0.25%) decreases from ~2.76 to 2.02 W/(m K) for $Pb_{1-x}Gd_xTe$ (x = 0.33%) at room temperature (Figure 3b). κ_{lat} for all the samples is found to decrease with increase in temperature. Low κ_{lat} of 0.78 W/(m K) is obtained at 735 K for $Pb_{1-x}Gd_xTe$ (x = 0.33%), which is due to a synergistic effect of off-centered Gd atom and phonon scattering due to the presence of low-energy localized optical phonon mode.

The peak thermoelectric figure of merit (zT) of ~1.2 at 783 K is observed for $Pb_{1-x}Gd_xTe$ (x = 0.33%), which is a result of the superior power factor and low κ_{lat} (Figure 3c). Further optimization is done on $Pb_{1-x}Gd_xTe$ (x = 0.33%) with I codoping. With subsequent Gd and I codoping, the band gap is found to increase from ~0.28 eV for $Pb_{1-x}Gd_xTe_{1-y}I_y$ (x = 0.33%, y = 0%) to ~0.33 eV for $Pb_{1-x}Gd_xTe_{1-y}I_y$ (x = 0.33%, y = 3%) at room temperature (Figure S9). I codoping is found to decrease the electrical conductivity but increases the S. Even 1 mol % I-doped $Pb_{1-x}Gd_xTe$ (x = 0.33%) reduces the room temperature σ value to 1400 S/cm compared to ~2484 S/cm for $Pb_{1-x}Gd_xTe$ (x = 0.33%) (Figure 4a). Additional incorporation of aliovalent I in the Te position results in further degradation of σ. $Pb_{1-x}Gd_xTe$ (x = 0.33%) doped with 2 and 3 mol % I shows σ values of ~1172 and 832 S/cm at room temperature, respectively (Figure 4a). This decrease in σ value might arise due to enhanced charge carrier scattering (Table S1). The σ of these I-doped $Pb_{1-x}Gd_xTe$ (x = 0.33%), however, decreases with increasing temperature, hence retaining the degenerate semiconductor properties of PbTe.

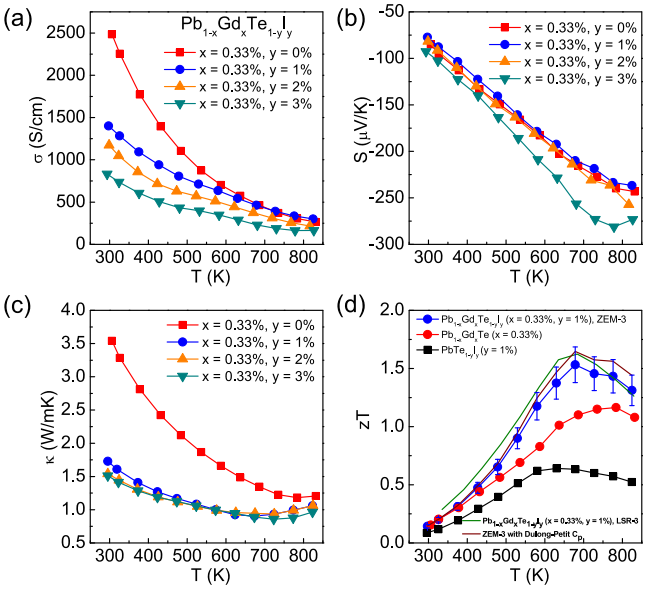

Figure 4. Temperature-dependent (a) electrical conductivity (σ), (b) Seebeck coefficient (S), and (c) total thermal conductivity (κ) of $Pb_{1-x}Gd_xTe_{1-y}I_y$. (d) zT vs T of $Pb_{1-x}Gd_xTe_{1-y}I_y$ compared with controlled individual doping in PbTe. High zT is validated by measuring the properties in different instruments.

The Seebeck coefficient for $Pb_{1-x}Gd_xTe_{1-y}I_y$ (x = 0.33%, y = 1−3%) increases with an increase in y and is in line with the electrical conductivity trend. The room temperature S value for $Pb_{1-x}Gd_xTe_{1-y}I_y$ (x = 0.33%, y = 1%) is −77 μV/K, which increases to −81 μV/K for $Pb_{1-x}Gd_xTe_{1-y}I_y$ (x = 0.33%, y = 2%) and finally up to −92 μV/K for $Pb_{1-x}Gd_xTe_{1-y}I_y$ (x = 0.33%, y = 3%) (Figure 4b). The |S| vs n Pisarenko plot (Figure 1d) shows that I doping does not perturb the conduction band effective m^* and it is only essential for optimizing the n-type carrier concentration (Table S1), thereby the S and σ values. S is found to increase almost linearly with an increase in temperature for all the samples. A high power factor of ~20.3 μW/(cm K^2) is found for $Pb_{1-x}Gd_xTe_{1-y}I_y$ (x = 0.33%, y = 1%) at 579 K and remains almost flat up to the measured maximum temperature (Figure S10).

The room temperature thermal conductivity of $Pb_{1-x}Gd_xTe_{1-y}I_y$ (x = 0.33%, y = 1−3%) decreases dramatically from 3.54 to 1.51 W/(m K) for y = 0% and y = 3%, respectively (Figure 4c). Such a decrease in total thermal conductivity is due to the combination of two effects: the first one being significant reduction in the κ_{el} and the other being phonon scattering due to additional point defect scattering from I doping. The κ_{lat} decreases from ~2.02 W/(m K) for $Pb_{1-x}Gd_xTe_{1-y}I_y$ (x = 0.33%, y = 0%) to ~0.78 W/(m K) for $Pb_{1-x}Gd_xTe_{1-y}I_y$ (x = 0.33%, y = 2%) at room temperature (Figure S11). The κ_{lat} reaches an ultralow value of 0.36 W/(m K) at ~630 K for $Pb_{1-x}Gd_xTe_{1-y}I_y$ (x = 0.33%, y = 1%), lying above the predicted lower limit κ_{diff} value of 0.157 W/(m K) (Figure S11).[52]

The maximum zT of 1.54 at 678 K for $Pb_{1-x}Gd_xTe_{1-y}I_y$ (x = 0.33%, y = 1%) (Figure 4d and Figure S12) was measured. This high zT is a result of the synergistic effect of Gd and I codoping, and this effect is found to increase the thermoelectric performance of the n-type PbTe as compared to their individual contributions, as shown in Figure 4d. The thermoelectric performance was further verified through repeated cycles and the electrical properties were verified using two different instruments (Figure S13). The peak zT using Ulvac Riko ZEM-3 and Linseis LSR-3 are found to be 1.54 at 678 K and 1.62 at 683 K, respectively (Figure 4d). Peak zT further improves to ~1.65 at 678 K (Figure 4d) if the thermal conductivity is estimated using heat capacity from Dulong-Petit limit of 0.15 J/(g K) like determined in other previous n-type PbTe based reports.[6,17,24,26] The high zT in the present system is comparable and even higher to other state of the art n-type PbTe materials. We have achieved a high zT_{ave} of 1.15 in the temperature range 423−823 K for $Pb_{1-x}Gd_xTe_{1-y}I_y$ (x = 0.33%, y = 1%).

In conclusion, Gd doping introduces a noninteracting flat conduction band in n-type PbTe, which increases its band effective mass (m^*). The presence of this nearly flat conduction band distorts the electronic DOS, which is beneficial for enhancing the Seebeck coefficient of n-type PbTe. |S| vs n Pisarenko plot reveals that the m^* increases from 0.35m_e to ~0.45m_e with an increase in Gd doping (from 0.25 to 0.75 mol %) for n-type PbTe. Gd is found to be favorable when it is locally off-centered from its parent position by ~0.21 Å along the [111] crystallographic direction in the PbTe

https://doi.org/10.1021/acsenergylett.1c00450
ACS Energy Lett. 2021, 6, 1625−1632

lattice, which creates significant lattice anharmonicity. Phonon dispersion reveals the presence of low-frequency nearly flat optical phonon mode and plays a pivotal role in scattering the heat carrying acoustic phonons, thus lowering its κ_{lat} to a low value. The high thermoelectric performance of Gd-doped PbTe is the result of the high power factor arising due to distortion of electronic DOS and the simultaneous low thermal conductivity due to Gd off-centering and enhanced scattering due to formation of low-energy localized phonon modes. Further improvement in the zT is obtained via I incorporation in $Pb_{1-x}Gd_xTe$ (x = 0.33%); 1 mol % I codoping shows a high peak zT of 1.65 at 678 K, and an impressive zT_{ave} of 1.15 is obtained in a broad temperature range of 423−823 K.

■ ASSOCIATED CONTENT

Supporting Information

The Supporting Information is available free of charge at https://pubs.acs.org/doi/10.1021/acsenergylett.1c00450.

Methods for synthesis and measurements of n-type doped PbTe samples and theoretical analysis; figures of powder XRD and band gap of Gd-doped PbTe (Figure S1), Gd-doping-dependent lattice parameter (Figure S2), FESEM image and EDAX color mapping (Figure S3), TEM images (Figure S4), PDOS and COHP (Figure S5), Eigen mode visualizations (Figure S6), phonon DOS and group velocities of phonon modes (Figure S7), PXRD of I- and Gd-codoped PbTe (Figure S8), band gap of I- and Gd-codoped PbTe (Figure S9), power factor for I- and Gd-codoped PbTe (Figure S10), κ_{lat} for I- and Gd-codoped PbTe (Figure S11), additional zT vs T plot (Figure S12), reproducibility data (Figure S13), thermal diffusivity, Lorentz number, and κ_{el} (Figure S14), theoretical C_v vs T plot (Figure S15), and transport properties of I doped PbTe (Figure S16); tables for carrier concentration (Table S1), speed of sound (Table S2), and some vibrational Eigen values (Table S3) (PDF)

■ AUTHOR INFORMATION

Corresponding Author

Kanishka Biswas − *New Chemistry Unit, Jawaharlal Nehru Centre for Advanced Scientific Research (JNCASR), Bangalore 560064, India; School of Advanced Materials and International Centre for Materials Science, Jawaharlal Nehru Centre for Advanced Scientific Research (JNCASR), Bangalore 560064, India;* orcid.org/0000-0001-9119-2455; Email: kanishka@jncasr.ac.in

Authors

Moinak Dutta − *New Chemistry Unit, Jawaharlal Nehru Centre for Advanced Scientific Research (JNCASR), Bangalore 560064, India*

Raju K. Biswas − *Theoretical Sciences Unit, Jawaharlal Nehru Centre for Advanced Scientific Research (JNCASR), Bangalore 560064, India*

Swapan K. Pati − *Theoretical Sciences Unit, Jawaharlal Nehru Centre for Advanced Scientific Research (JNCASR), Bangalore 560064, India; School of Advanced Materials and International Centre for Materials Science, Jawaharlal Nehru Centre for Advanced Scientific Research (JNCASR), Bangalore 560064, India;* orcid.org/0000-0002-5124-7455

Complete contact information is available at: https://pubs.acs.org/10.1021/acsenergylett.1c00450

Notes

The authors declare no competing financial interest.

■ ACKNOWLEDGMENTS

K.B. acknowledge the DST-BRICS project (DST/IMRD/BRICS/BNEAT/2018G) and SERB, DST (CRG/2019/001306), for funding this work. M.D. and R.K.B. thank the University Grants Commission (UGC) for the research fellowship. S.K.P. acknowledges SERB, a JC Bose Fellowship, and DST for the financial support.

■ REFERENCES

(1) Tan, G.; Zhao, L.-D.; Kanatzidis, M. G. Rationally Designing High-Performance Bulk Thermoelectric Materials. *Chem. Rev.* **2016**, *116*, 12123−12149.

(2) Shi, X.-L.; Zou, J.; Chen, Z.-G. Advanced Thermoelectric Design: From Materials and Structures to Devices. *Chem. Rev.* **2020**, *120*, 7399−7515.

(3) Xiao, Y.; Zhao, L.-D. Seeking new, highly effective thermoelectrics. *Science* **2020**, *367*, 1196−1197.

(4) Roychowdhury, S.; Ghosh, T.; Arora, R.; Samanta, M.; Xie, L.; Singh, N. K.; Soni, A.; He, J.; Waghmare, U. V.; Biswas, K. Enhanced atomic ordering leads to high thermoelectric performance in $AgSbTe_2$. *Science* **2021**, *371*, 722−727.

(5) Jiang, B.; Yu, Y.; Cui, J.; Liu, X.; Xie, L.; Liao, J.; Zhang, Q.; Huang, Y.; Ning, S.; Jia, B.; Zhu, B.; Bai, S.; Chen, L.; Pennycook, S. J.; He, J. High-entropy-stabilized chalcogenides with high thermoelectric performance. *Science* **2021**, *371*, 830−834.

(6) Xiao, Y.; Wu, H.; Cui, J.; Wang, D.; Fu, L.; Zhang, Y.; Chen, Y.; He, J.; Pennycook, S. J.; Zhao, L.-D. Realizing high performance n-type PbTe by synergistically optimizing effective mass and carrier mobility and suppressing bipolar thermal conductivity. *Energy Environ. Sci.* **2018**, *11*, 2486−2495.

(7) Tan, G.; Stoumpos, C. C.; Wang, S.; Bailey, T. P.; Zhao, L.-D.; Uher, C.; Kanatzidis, M. G. Subtle Roles of Sb and S in Regulating the Thermoelectric Properties of N-Type PbTe to High Performance. *Adv. Energy Mater.* **2017**, *7*, 1700099.

(8) Pei, Y.; Shi, X.; LaLonde, A.; Wang, H.; Chen, L.; Snyder, G. J. Convergence of electronic bands for high performance bulk thermoelectrics. *Nature* **2011**, *473*, 66−69.

(9) Jood, P.; Male, J. P.; Anand, S.; Matsushita, Y.; Takagiwa, Y.; Kanatzidis, M. G.; Snyder, G. J.; Ohta, M. Na Doping in PbTe: Solubility, Band Convergence, Phase Boundary Mapping, and Thermoelectric Properties. *J. Am. Chem. Soc.* **2020**, *142*, 15464−15475.

(10) Sarkar, D.; Ghosh, T.; Banik, A.; Roychowdhury, S.; Sanyal, D.; Biswas, K. Highly Converged Valence Bands and Ultralow Lattice Thermal Conductivity for High-Performance SnTe Thermoelectrics. *Angew. Chem., Int. Ed.* **2020**, *59*, 11115−11122.

(11) You, L.; Zhang, J.; Pan, S.; Jiang, Y.; Wang, K.; Yang, J.; Pei, Y.; Zhu, Q.; Agne, M. T.; Snyder, G. J.; Ren, Z.; Zhang, W.; Luo, J. Realization of higher thermoelectric performance by dynamic doping of copper in n-type PbTe. *Energy Environ. Sci.* **2019**, *12*, 3089−3098.

(12) Qin, C.; Cheng, L.; Xiao, Y.; Wen, C.; Ge, B.; Li, W.; Pei, Y. Substitutions and dislocations enabled extraordinary n-type thermoelectric PbTe. *Mater. Today Phys.* **2021**, *17*, 100355.

(13) Heremans, J. P.; Jovovic, V.; Toberer, E. S.; Saramat, A.; Kurosaki, K.; Charoenphakdee, A.; Yamanaka, S.; Snyder, G. J. Enhancement of Thermoelectric Efficiency in PbTe by Distortion of the Electronic Density of States. *Science* **2008**, *321*, 554−557.

(14) Banik, A.; Shenoy, U. S.; Saha, S.; Waghmare, U. V.; Biswas, K. High Power Factor and Enhanced Thermoelectric Performance of SnTe-$AgInTe_2$: Synergistic Effect of Resonance Level and Valence Band Convergence. *J. Am. Chem. Soc.* **2016**, *138*, 13068−13075.

(15) He, J.; Girard, S. N.; Kanatzidis, M. G.; Dravid, V. P. Microstructure-Lattice Thermal Conductivity Correlation in Nanostructured $PbTe_{0.7}S_{0.3}$ Thermoelectric Materials. *Adv. Funct. Mater.* **2010**, *20*, 764−772.
(16) Zhao, L.-D.; Hao, S.; Lo, S.-H.; Wu, C.-I.; Zhou, X.; Lee, Y.; Li, H.; Biswas, K.; Hogan, T. P.; Uher, C.; Wolverton, C.; Dravid, V. P.; Kanatzidis, M. G. High Thermoelectric Performance via Hierarchical Compositionally Alloyed Nanostructures. *J. Am. Chem. Soc.* **2013**, *135*, 7364−7370.
(17) Xiao, Y.; Wu, H.; Li, W.; Yin, M.; Pei, Y.; Zhang, Y.; Fu, L.; Chen, Y.; Pennycook, S. J.; Huang, L.; He, J.; Zhao, L.-D. Remarkable Roles of Cu To Synergistically Optimize Phonon and Carrier Transport in n-Type PbTe-Cu_2Te. *J. Am. Chem. Soc.* **2017**, *139*, 18732−18738.
(18) Wang, S.; Xiao, Y.; Chen, Y.; Peng, S.; Wang, D.; Hong, T.; Yang, Z.; Sun, Y.; Gao, X.; Zhao, L.-D. Hierarchical structures lead to high thermoelectric performance in $Cu_{m+n}Pb_{100}Sb_mTe_{100}Se_{2m}$ (CLAST). *Energy Environ. Sci.* **2021**, *14*, 451−461.
(19) Luo, Z.-Z.; Zhang, X.; Hua, X.; Tan, G.; Bailey, T. P.; Xu, J.; Uher, C.; Wolverton, C.; Dravid, V. P.; Yan, Q.; Kanatzidis, M. G. High Thermoelectric Performance in Supersaturated Solid Solutions and Nanostructured n-Type PbTe-GeTe. *Adv. Funct. Mater.* **2018**, *28*, 1801617.
(20) Luo, Z.-Z.; Cai, S.; Hao, S.; Bailey, T. P.; Su, X.; Spanopoulos, I.; Hadar, I.; Tan, G.; Luo, Y.; Xu, J.; Uher, C.; Wolverton, C.; Dravid, V. P.; Yan, Q.; Kanatzidis, M. G. High Figure of Merit in Gallium-Doped Nanostructured n-Type PbTe-*x*GeTe with Midgap States. *J. Am. Chem. Soc.* **2019**, *141*, 16169−16177.
(21) Li, J.; Zhang, X.; Chen, Z.; Lin, S.; Li, W.; Shen, J.; Witting, I. T.; Faghaninia, A.; Chen, Y.; Jain, A.; Chen, L.; Snyder, G. J.; Pei, Y. Low-Symmetry Rhombohedral GeTe Thermoelectrics. *Joule* **2018**, *2*, 976−987.
(22) Roychowdhury, S.; Biswas, K. Slight Symmetry Reduction in Thermoelectrics. *Chem.* **2018**, *4*, 939−942.
(23) Dutta, M.; Ghosh, T.; Biswas, K. Electronic structure modulation strategies in high-performance thermoelectrics. *APL Mater.* **2020**, *8*, 040910.
(24) Fu, L.; Yin, M.; Wu, D.; Li, W.; Feng, D.; Huang, L.; He, J. Large enhancement of thermoelectric properties in n-type PbTe via dual-site point defects. *Energy Environ. Sci.* **2017**, *10*, 2030−2040.
(25) Roychowdhury, S.; Biswas, R. K.; Dutta, M.; Pati, S. K.; Biswas, K. Phonon Localization and Entropy-Driven Point Defects Lead to Ultralow Thermal Conductivity and Enhanced Thermoelectric Performance in $(SnTe)_{1-2x}(SnSe)_x(SnS)_x$. *ACS Energy Lett.* **2019**, *4*, 1658−1662.
(26) Zhang, J.; Wu, D.; He, D.; Feng, D.; Yin, M.; Qin, X.; He, J. Extraordinary Thermoelectric Performance Realized in n-Type PbTe through Multiphase Nanostructure Engineering. *Adv. Mater.* **2017**, *29*, 1703148.
(27) Liu, S.; Yu, Y.; Wu, D.; Xu, X.; Xie, L.; Chao, X.; Bosman, M.; Pennycook, S. J.; Yang, Z.; He, J. Coherent Sb/CuTe Core/Shell Nanostructure with Large Strain Contrast Boosting the Thermoelectric Performance of n-Type PbTe. *Adv. Funct. Mater.* **2021**, *31*, 2007340.
(28) Lee, M. H.; Yun, J. H.; Kim, G.; Lee, J. E.; Park, S.-D.; Reith, H.; Schierning, G.; Nielsch, K.; Ko, W.; Li, A.-P.; Rhyee, J.-S. Synergetic Enhancement of Thermoelectric Performance by Selective Charge Anderson Localization−Delocalization Transition in n-Type Bi-Doped PbTe/Ag_2Te Nanocomposite. *ACS Nano* **2019**, *13*, 3806−3815.
(29) Biswas, K.; He, J.; Blum, I. D.; Wu, C. I.; Hogan, T. P.; Seidman, D. N.; Dravid, V. P.; Kanatzidis, M. G. High-performance bulk thermoelectrics with all-scale hierarchical architectures. *Nature* **2012**, *489*, 414−418.
(30) Zhao, L. D.; Wu, H. J.; Hao, S. Q.; Wu, C. I.; Zhou, X. Y.; Biswas, K.; He, J. Q.; Hogan, T. P.; Uher, C.; Wolverton, C.; Dravid, V. P.; Kanatzidis, M. G. All-scale hierarchical thermoelectrics: MgTe in PbTe facilitates valence band convergence and suppresses bipolar thermal transport for high performance. *Energy Environ. Sci.* **2013**, *6*, 3346−3355.
(31) Liu, H.; Chen, Z.; Tang, J.; Zhong, Y.; Guo, X.; Zhang, F.; Ang, R. High Quality Factor Enabled by Multiscale Phonon Scattering for Enhancing Thermoelectrics in Low-Solubility n-Type PbTe−Cu_2Te Alloys. *ACS Appl. Mater. Interfaces* **2020**, *12*, 52952−52958.
(32) Jana, M. K.; Biswas, K. Crystalline Solids with Intrinsically Low Lattice Thermal Conductivity for Thermoelectric Energy Conversion. *ACS Energy Lett.* **2018**, *3*, 1315−1324.
(33) Xiao, Y.; Zhao, L.-D. Charge and phonon transport in PbTe-based thermoelectric materials. *npj Quantum Mater.* **2018**, *3*, 55.
(34) Tan, G.; Shi, F.; Hao, S.; Zhao, L.-D.; Chi, H.; Zhang, X.; Uher, C.; Wolverton, C.; Dravid, V. P.; Kanatzidis, M. G. Non-equilibrium processing leads to record high thermoelectric figure of merit in PbTe−SrTe. *Nat. Commun.* **2016**, *7*, 12167.
(35) Zhong, Y.; Tang, J.; Liu, H.; Chen, Z.; Lin, L.; Ren, D.; Liu, B.; Ang, R. Optimized Strategies for Advancing n-Type PbTe Thermoelectrics: A Review. *ACS Appl. Mater. Interfaces* **2020**, *12*, 49323−49334.
(36) Qin, Y.; Xiao, Y.; Zhao, L.-D. Carrier mobility does matter for enhancing thermoelectric performance. *APL Mater.* **2020**, *8*, 010901.
(37) LaLonde, A. D.; Pei, Y.; Snyder, G. J. Reevaluation of $PbTe_{1-x}I_x$ as high performance n-type thermoelectric material. *Energy Environ. Sci.* **2011**, *4*, 2090−2096.
(38) Yang, Z.; Wang, S.; Sun, Y.; Xiao, Y.; Zhao, L.-D. Enhancing thermoelectric performance of n-type PbTe through separately optimizing phonon and charge transport properties. *J. Alloys Compd.* **2020**, *828*, 154377.
(39) Pei, Y.; Lensch-Falk, J.; Toberer, E. S.; Medlin, D. L.; Snyder, G. J. High Thermoelectric Performance in PbTe Due to Large Nanoscale Ag_2Te Precipitates and La Doping. *Adv. Funct. Mater.* **2011**, *21*, 241−249.
(40) Hsu, K. F.; Loo, S.; Guo, F.; Chen, W.; Dyck, J. S.; Uher, C.; Hogan, T.; Polychroniadis, E. K.; Kanatzidis, M. G. Cubic $AgPb_mSbTe_{2+m}$: Bulk Thermoelectric Materials with High Figure of Merit. *Science* **2004**, *303*, 818−821.
(41) Pei, Y.; LaLonde, A. D.; Wang, H.; Snyder, G. J. Low effective mass leading to high thermoelectric performance. *Energy Environ. Sci.* **2012**, *5*, 7963−7969.
(42) Zayachuk, D. M.; Ivanchuk, D. D.; Ivanchuk, R. D.; Maslyanchuk, S. S.; Mikityuk, V. I. The Effect of Gadolinium Doping on the Physical Properties of Lead Telluride. *phys. stat. sol. (a)* **1990**, *119*, 215−219.
(43) Nouneh, K.; Plucinski, K.; Bakasse, M.; Kityk, I. Thermoelectrical properties and optical third harmonic generation of Gd-doped PbTe. *J. Mater. Sci.* **2007**, *42*, 6847−6853.
(44) Isaacs, E. B.; Wolverton, C. Remarkable thermoelectric performance in $BaPdS_2$ via pudding-mold band structure, band convergence, and ultralow lattice thermal conductivity. *Phys. Rev. Mater.* **2019**, *3*, 015403.
(45) Mori, K.; Sakakibara, H.; Usui, H.; Kuroki, K. Ideal band shape in the potential thermoelectric material $CuAlO_2$: Comparison to Na_xCoO_2. *Phys. Rev. B: Condens. Matter Mater. Phys.* **2013**, *88*, 075141.
(46) Sastri, V. S.; Bünzli, J.-C.; Rao, V. R.; Rayudu, G. V. S.; Perumareddi, J. R. Structural Chemistry of Lanthanide Complexes. *Modern Aspects of Rare Earths and Their Complexes*; Elsevier: Amsterdam, 2003; Chapter 5, pp 375−422.
(47) Luo, Z.-Z.; Hao, S.; Zhang, X.; Hua, X.; Cai, S.; Tan, G.; Bailey, T. P.; Ma, R.; Uher, C.; Wolverton, C.; Dravid, V. P.; Yan, Q.; Kanatzidis, M. G. Soft phonon modes from off-center Ge atoms lead to ultralow thermal conductivity and superior thermoelectric performance in n-type PbSe-GeSe. *Energy Environ. Sci.* **2018**, *11*, 3220−3230.
(48) Sarkar, S.; Hua, X.; Hao, S.; Zhang, X.; Bailey, T. P.; Slade, T. J.; Yasaei, P.; Korkosz, R. J.; Tan, G.; Uher, C.; Dravid, V. P.; Wolverton, C.; Kanatzidis, M. G. Dissociation of GaSb in n-Type PbTe: off-Centered Gallium Atom and Weak Electron−Phonon

https://doi.org/10.1021/acsenergylett.1c00450
ACS Energy Lett. 2021, 6, 1625−1632

Coupling Provide High Thermoelectric Performance. *Chem. Mater.* **2021**, *33*, 1842−1851.
(49) Ikeda, M. S.; Euchner, H.; Yan, X.; Tomeš, P.; Prokofiev, A.; Prochaska, L.; Lientschnig, G.; Svagera, R.; Hartmann, S.; Gati, E.; Lang, M.; Paschen, S. Kondo-like phonon scattering in thermoelectric clathrates. *Nat. Commun.* **2019**, *10*, 887.
(50) Li, W.; Mingo, N. Ultralow lattice thermal conductivity of the fully filled skutterudite $YbFe_4Sb_{12}$ due to the flat avoided-crossing filler modes. *Phys. Rev. B: Condens. Matter Mater. Phys.* **2015**, *91*, 144304.
(51) Pal, K.; Xia, Y.; He, J.; Wolverton, C. Intrinsically Low Lattice Thermal Conductivity Derived from Rattler Cations in an $AMM'Q_3$ Family of Chalcogenides. *Chem. Mater.* **2019**, *31*, 8734−8741.
(52) Agne, M. T.; Hanus, R.; Snyder, G. J. Minimum thermal conductivity in the context of diffuson-mediated thermal transport. *Energy Environ. Sci.* **2018**, *11*, 609−616.

https://doi.org/10.1021/acsenergylett.1c00450
ACS Energy Lett. 2021, 6, 1625−1632